Acta Astronautica 221 (2024) 142–154

Contents lists available at ScienceDirect

Acta Astronautica

journal homepage: www.elsevier.com/locate/actaastro

Poly(vinyl alcohol) gels cross-linked by boric acid for radiation protection of astronauts

Lucia Lambertini [a], Giuseppe Coccarelli [b], Elisa Toto [b], Maria Gabriella Santonicola [b,**], Susanna Laurenzi [a,*]

[a] Department of Astronautical Electrical and Energy Engineering, Sapienza University of Rome, Via Salaria 851-881, 00138, Rome, Italy
[b] Department of Chemical Engineering Materials Environment, Sapienza University of Rome, Via del Castro Laurenziano 7, 00161, Rome, Italy

ARTICLE INFO

Keywords:
Cross-linked gels
Mechanical behavior
Space radiation shielding
Space suit

ABSTRACT

Gels are soft materials composed of hydrophilic polymers cross-linked in water by physical or chemical bonds. Due to their lightweight and water-rich nature, these materials find application in various fields, including the space environment, for radiation protection purposes. In fact, thanks to their high hydrogen content, gels exhibit significant radiation stopping power, resulting in reduced fragmentation of incident particles. This suggests their potential utility in shielding electronic devices and safeguarding astronauts' health. In this work, cross-linked gels based on poly(vinyl alcohol) (PVA) and boric acid (BA) were fabricated and their properties were investigated using different experimental and modeling techniques. The effect of parameters, such as time and temperature, used for fabricating the PVA/BA gels is assessed. Fourier transform infrared spectroscopy (FTIR) was employed to evaluate the ability of BA to form hybrid interpolymeric bonds with PVA macromolecules. To understand the thermo-mechanical properties and viscoelastic behavior of these gels, dynamic mechanical analysis (DMA) in compression mode was performed. The shielding properties were evaluated in different space radiation environments considering galactic cosmic rays, solar particle events, and low earth orbit radiation using deterministic transport codes. The High charge (Z) and Energy TRaNsport (HZETRN) code was employed to create different cross sections as first output for the selected materials, and then, propagate and transport the ionizing radiation inside the materials. The results highlight several advantages of PVA/BA gels fabricated at room temperature without heat treatments. Firstly, the incorporation of BA allows for a slight increase in water content compared to gels produced without the crosslinker. Additionally, an examination of elastic moduli reveals improved mechanical properties exhibiting approximately twice the elastic modulus of PVA gels. Moreover, the analysis of dosimetry quantities suggests that the radiation protection effectiveness of these gels is comparable to that of pure water, while heat-treated PVA/BA gels exhibit a reduced water content resulting in decreased shielding properties and decreased flexibility. Consequently, PVA/BA gels realized at room temperature appear to be the optimal material between PVA gels and the heat-treated counterparts, making them well-suited for integration into astronaut personal protective equipment.

1. Introduction

One of the foremost challenges in space missions continues to be the development of spacecraft designs capable of effective radiation shielding, particularly for human crews. This is because charged particles present in space environments pose a significant risk of increasing the likelihood of mission failure [1]. In terms of protective techniques, the implementation of passive shielding for reducing radiation exposure is of particular interest [2,3]. Through simulations conducted on various protective materials, hydrogen-rich materials, especially liquid water, methane, hydrogen and polyethylene, have been considered as optimal at reducing radiation absorbed dose due to their high stopping power [4–8]. This result was confirmed from experiments carried out by the Italian Space Agency (ASI) as a part of the Personal Radiation Shielding for intErplanetary missiOns (PERSEO) project [9]. These experiments demonstrated the shielding effectiveness of panels containing water

* Corresponding author.
** Corresponding author.
E-mail addresses: mariagabriella.santonicola@uniroma1.it (M.G. Santonicola), susanna.laurenzi@uniroma1.it (S. Laurenzi).

https://doi.org/10.1016/j.actaastro.2024.05.020
Received 15 January 2024; Received in revised form 2 May 2024; Accepted 13 May 2024
Available online 14 May 2024

within spacecraft or, more broadly, within habitats on the International Space Station (ISS).

Furthermore, shielding effectiveness of polymer-based materials was demonstrated for protection of spacecraft components, as they offer lightweight solutions with customizable mechanical, thermal, and electrical properties. By incorporating appropriate fillers into polymers, their radiation shielding capabilities can be greatly enhanced [10,11]. Zhang et al. proposed a composite material comprising ultra-high molecular weight polyethylene fibers (UPEF), boron nitride (BN), and polyurethane (PU) for shielding against neutron radiation [12]. Zaccardi et al. fabricated multifunctional nanocomposites using medium-density polyethylene (MDPE) loaded with multi-walled carbon nanotubes (MWCNTs), graphene nanopatterns (GNPs), and MWCNT/GNP hybrid fillers for proton irradiation [13]. Additionally, a multilayer composite material was developed by alternating layers of high-density polyethylene/hexagonal boron nitride (HDPE/hBN) and low-density polyethylene (LDPE) [14]. Subsequent evaluation of the neutron shielding capability of these PE/hBN composites was conducted following neutron irradiation experiments. Polyimide-based materials exhibit potential as neutron moderators due to their composition of carbon, hydrogen, nitrogen, and oxygen. Their radiation-shielding effectiveness has been notably augmented using nanomaterials like bismuth oxide and boron nitride. Among these fillers, bismuth oxide (Bi_2O_3) demonstrates efficacy against γ-ray exposure [15]. In a study, a polyimide matrix was enriched with gadolinium oxide (Gd_2O_3) and hexagonal boron nitride (hBN) nanoparticles, offering shielding properties against both neutrons and γ-rays [16]. Furthermore, polyimide-hexagonal boron nitride (PI-hBN) nanocomposites were produced via direct forming technology (DF) to enhance radiation-shielding properties [17].

Over the years, numerous efforts have been dedicated to incorporating water into the spacesuits worn by astronauts, primarily for its shielding capabilities and as part of the cooling system [18,19]. The development of spacesuits remains a significant area of research, aimed at ensuring the reliability and safety of astronauts. This encompasses various aspects, including human-suit interactions, movement optimization, injury assessment, and radiation protection [20]. Notably, recent advancements include the design of a new hip joint and its coupling mechanism, featuring five links for the joint and the femur-thigh components, along with six joints within the coupling mechanism [21]. On the thermal front, lightweight hybrid aerogels, combining polyimide and polystyrene-silica, have been developed as insulation materials for spacesuits [22–24]. Furthermore, while PVA/BA gels have primarily been studied and explored for their radiation shielding capabilities in nuclear reactors due to their content of the ^{10}B isotope renowned for its neutron-absorbing properties [25], their potential application in the space field for radiation shielding is gaining prominence. This is because achieving a substantial hydrogen and boron content is essential for minimizing the damage caused by ionizing radiation to both astronauts and electronic devices, making cross-linked gels attractive materials for radiation shielding applications in space.

To date astronauts are protected during their extra-vehicular activities by wearing spacesuits made of multiple layers, whose detailed breakdown is reported in Fig. 1 [20,22]. The outer cover, constructed from ortho-fabric, serves as the initial defense against micrometeorite impacts. Moving inward, a multi-layered insulator comprising aluminized Mylar and a Dacron restraint is utilized for thermal insulation. Finally, the innermost layer comprises a pressure bladder garment (PBG) and a liquid cooling and ventilation garment (LCVG), designed to maintain a stable internal suit temperature.

The PBG is crafted from urethane-coated nylon, while the LCVG features an interior with nylon and water tubes running through it. Notably, the nylon fabric wicks away moisture and sweat, ensuring the astronaut's comfort, while the water tubes regulate temperature. Given that gels are inherently hydrophilic materials capable of fulfilling both these functions, it is worth considering the replacement of one of the materials in the PBG or LCVG with cross-linked gels to explore potential

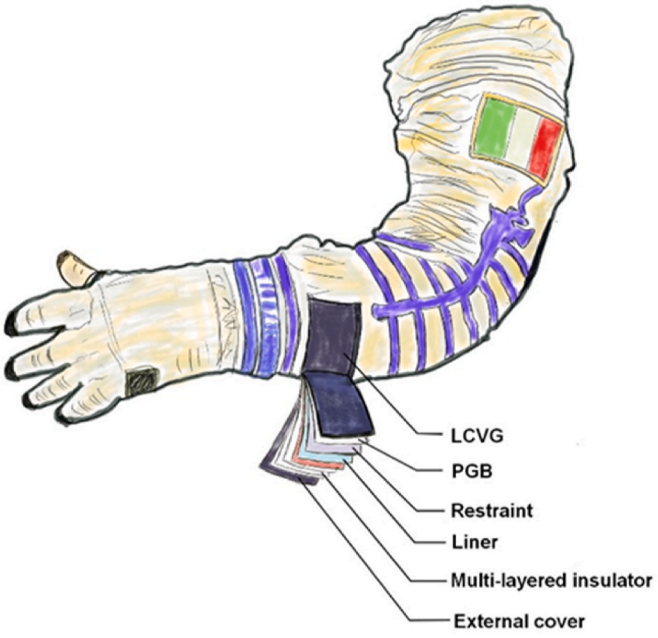

Fig. 1. Representative scheme of spacesuits with breakdown of multilayer structure.

enhancements in radiation protection.

Polymer gels consist of an elastic network of cross-linked polymers with water that is retained by the chain of polymer molecules filling the interstitial space [26]. These gel materials can be categorized as either natural or synthetic. Natural gels are composed of naturally occurring polymers, primarily polysaccharides, while synthetic gels are produced from engineered polymers to attain specific properties, such as a high affinity for water and greater resistance to degradation compared to natural polymers [26–29]. Synthetic polymer gels, in addition to being biocompatible, exhibit superior characteristics compared to their natural counterparts, including enhanced mechanical strength, rendering them valuable for applications in science and technology [27,30–32]. Furthermore, the remarkable attributes of versatility, softness, and flexibility exhibited by cross-linked polymer gels have steadily peaked increasing interest over the past few decades. These characteristics have positioned these gels as highly sought-after materials for diverse applications, spanning from the food and chemical industries to pharmaceuticals and biomedicine [33–37].

Depending on the type of polymer, gels can form through two primary types of crosslinking. Physical cross-linking, also known as self-assembled gels, takes place without the involvement of covalent bonds, often utilizing methods that eliminate the necessity for cross-linking agents [38]. These gels are typically reversible, as their temporary junctions and interactions can be disrupted with slight alterations in conditions or by applying stress to the gel matrix. In general, this technique allows cross-linking by hydrophobic or ionic interactions and by hydrogen bonds. It has been observed that hydrophobic interactions are relatively stronger than the Vander Waal bond and the hydrogen bond [39]. On the other hand, utilizing crosslinkers enables the creation of chemically cross-linked gels, which incorporate covalent bonds within the polymer chain [40]. It is commonly achieved through reactions like polymerization, oxidation, or other cross-linking mechanisms. This process not only strengthens the gel network but also enhances its stability and durability, rendering it suitable for prolonged applications.

Among synthetic polymers, PVA stands out as one of the most extensively employed materials due to its remarkable properties such as biodegradability, biocompatibility, lightweight nature, and low toxicity [41]. Notably, the hydroxyl groups (-OH) present in the primary

polymer chain establish hydrogen bonds with water functional groups, leading to a high degree of crystallinity and solubility [42–45]. One of the most widely adopted techniques involves physical crosslinking, achieved through a series of freezing and thawing (FT) cycles of aqueous PVA solutions. During this process, hydrogen bonds form between the polymer chain and the water, contributing to gel formation [46–48]. Generally, samples fabricated using this technique demonstrate autonomous self-healing properties. Upon comparison of gels obtained through various FT cycles (ranging from 1 to 3), it was noted that with an increase in the number of FT cycles, the self-healing capability of the gels decreased, while the elastic modulus increased [46]. Additionally, the process of chemical cross-linking or ionic cross-linking has been utilized. This method employs a cross-linking agent dispersed in water to facilitate the formation of chemical or ionic gels through condensation reactions between water and polymers [25,49–51]. Different heat treatments could be used for gelation process when considering chemical or ionic cross-linking. One of interest is the annealing consisting in heating samples at 100 °C. In comparison to PVA gel prepared at room temperature, this method significantly enhances mechanical properties, resulting in higher tensile stress, approximately 1.7 times greater than the gel prepared at room temperature [43].

Boric acid (BA) is a versatile cross-linking agent, which offers the potential to enhance mechanical properties and increase the water-retention capacity of gels and films [49,52–54]. It is well known that BA can form hybrid interpolymeric bonds with PVA molecules [55–58]. In particular, Chen et al. have suggested a di-diol type bond due to the crosslink reaction of PVA with borate ion [58]. Subsequently, Prosanov et al. provided further evidence of PVA forming coordinative bonds with BA, employing various techniques such as Raman spectroscopy and quantum mechanical calculations on Gaussian 09 software [55]. Initial testing has been conducted on these materials, with a primary assessment using differential scanning calorimetry (DSC) to investigate the melting behavior of the gels. Interestingly, it was observed that the melting temperature decreases as the percentage of BA increases [54]. Additionally, rheological properties have revealed that viscosity is strongly influenced by both BA concentration and temperature. Specifically, viscosity decreases to a minimum value at 70°C and then increases again between 70°C and 100°C. Furthermore, in terms of BA content, viscosity increases as the proportion of the cross-linking agent rises [59,60].

In this work, PVA-based gels were fabricated using BA as a cross-linking, and their properties were investigated through a range of experimental methods. BA was chosen as a cross-linking agent to enhance both the mechanical strength and radiation shielding capabilities of the gels. This resulted in the development of cross-linked PVA/BA gels with superior features in terms of overall volume, weight, and radiation shielding efficacy when compared to the liquid water garments currently employed in space missions. The study was conducted in several stages. Initially, we determine the optimal percentage of PVA required to create the gels by measuring the water content of samples containing 10–40 wt% of polymer over varying evaporation times. Next, we assess the increased swelling properties of PVA/BA gels compared to those composed of neat PVA by quantifying the amount of water retained. To investigate the presence of coordinative bonds in the PVA-BA complex, Fourier transform infrared spectroscopy (FTIR) is employed. The viscoelastic behavior of these materials is evaluated in terms of storage modulus and glass transition temperature by dynamic mechanical analysis (DMA). The radiation shielding capabilities of these gels are assessed using the deterministic transport code (HZETRN2020) provided by NASA. This analysis utilizes experimental data on water content and density of the gels as input. The results obtained are then used to assess the potential utility of these cross-linked PVA/BA gels as radiation shielding materials in space environments. Specifically, these gels could be applied as thin layers within spacesuits, offering advantages such as reduced weight and improved shielding effectiveness compared to the materials currently employed in the PERSEO project.

2. Experimental

2.1. Materials

The following products were purchased from Sigma-Aldrich (Milan, Italy) and used as received: partially hydrolyzed polyvinyl alcohol with a molecular weight of 30000 Da and density $\rho = 1.3$ g/cm^3 (product number 8438680100); boric acid (product number B0394). Ultrapure water with resistivity 18.2 MΩ-cm was produced by a Direct-Q3 UV purification system (Millipore, Molsheim, France).

2.2. Fabrication of PVA/BA gels

The cross-linked gels were fabricated by the following process. First, aqueous solutions of PVA were prepared by stirring the polymer powder for 1 h at a temperature of 80 °C. The PVA gels were obtained by dripping the solutions into molds and storing them at room temperature for 72 h. To determine the optimal PVA concentration, four different concentrations (0.1, 0.2, 0.3, 0.4 g/mL) were used, and the water content of the samples was evaluated over various evaporation times. Subsequently, PVA/BA gels were produced using the identified optimal PVA concentration (0.3 g/mL). This was achieved by introducing an additional step. A BA stock solution (5 wt%) was prepared by stirring BA in water at 40 °C for 20 min. An aliquot of the BA stock was then added to the PVA aqueous solution, resulting in a final solution containing 30 wt% of PVA and 1.4 wt% of BA. The PVA/BA gels were created by depositing the solutions into glass molds and storing them at room temperature for 72 h (referred to as treatment T0). Additional PVA/BA gels were prepared using specific heat treatments: one fabricated with a cycle at 23 °C for 24 h, followed by 80 °C for 45 min, and then at 23 °C for 72 h (referred to as treatment T1), and one gel fabricated with a cycle of 23 °C for 24 h, followed by 80 °C for 1.5 h, and then at 23 °C for 72 h (referred to as treatment T2). Samples obtained using the T2 heat treatment were sealed and stored at room temperature for 4 months to evaluate the aging effect on the water content and mechanical properties (referred to as treatment T2-A). Gels were named based on the heat treatment used, as outlined in Table 1. Fig. 2 shows the fabrication process of gel samples produced through the heat treatments (T0, T1, T2) with the reaction scheme of PVA and BA.

2.3. Characterization methods

To assess the swelling behavior and water content, the samples were prepared by cutting them into uniform strips measuring 0.5 cm × 0.5 cm. These strips were weighed and subsequently dried in an oven at a temperature of 50 °C for a duration of 24 h. Following the completion of the drying process, the gel strips were re-weighed to determine the total water evaporation. The swelling ratio (S) and water content (WC) are calculated using Eqs. (1) and (2), respectively [61]:

$$S = \frac{W_h}{W_d} \tag{1}$$

$$WC = \frac{W_h - W_d}{W_h} \times 100 \tag{2}$$

Table 1
PVA and PVA/BA gels classification based on the heat treatment used.

Samples	Heat treatment
PVA-T0	23 °C, 72 h (**T0**)
PVA/BA-T0	23 °C, 72 h (**T0**)
PVA/BA-T1	23 °C, 24 h + 80 °C, 45 min + 23 °C, 72 h (**T1**)
PVA/BA-T2	23 °C, 24 h + 80 °C, 1.5 h + 23 °C, 72 h (**T2**)
PVA/BA-T2-A	23 °C, 24 h + 80 °C, 1.5 h + 23 °C, 72 h + aging, 4 months (**T2-A**)

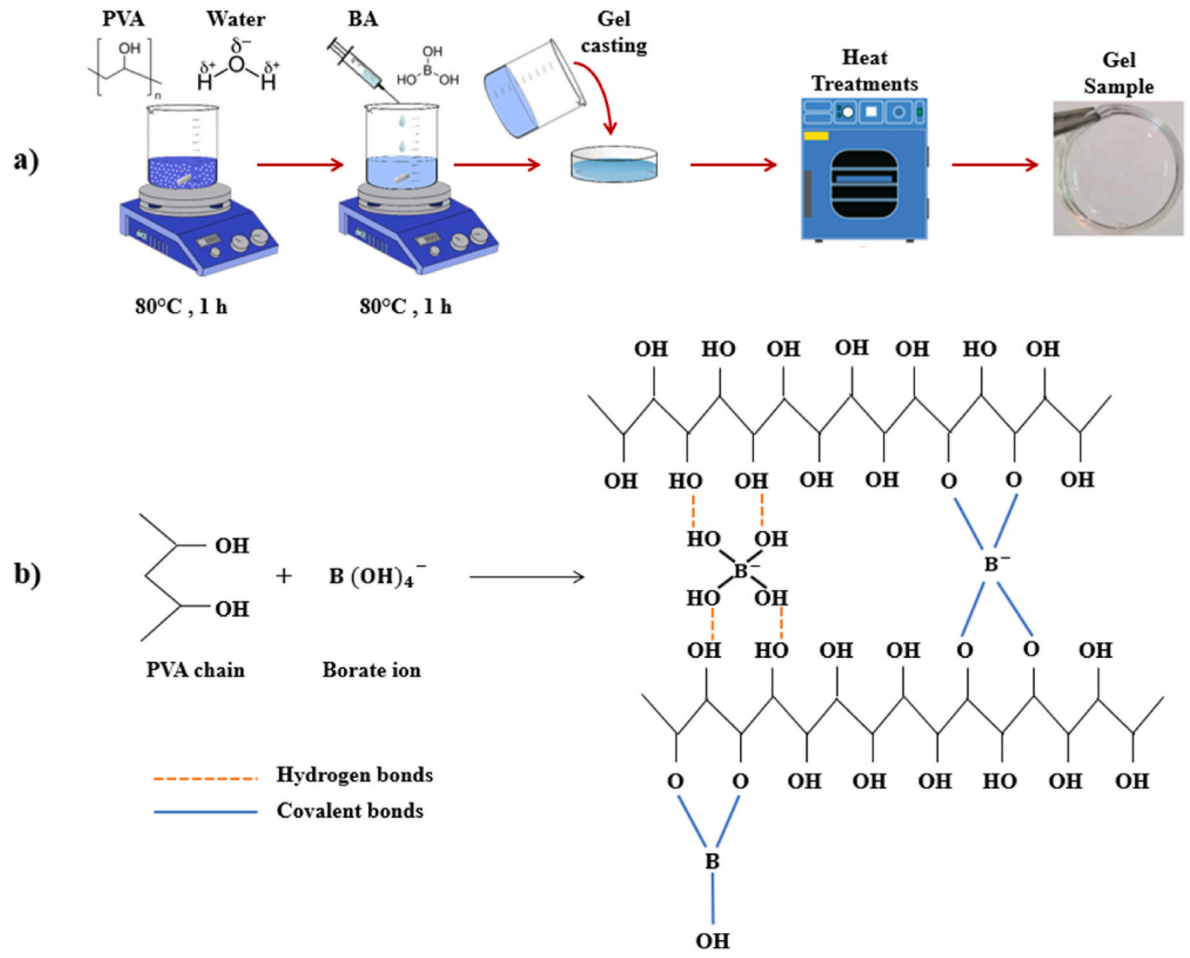

Fig. 2. Representative scheme of a) fabrication process and b) cross-linking reaction of PVA/BA gels.

where W_h is the weight of the hydrated gel and W_d its weight after complete drying.

A Nicolet Summit FTIR spectrometer (Thermo Fisher Scientific, Waltham, MA, USA) with a zinc selenide ATR accessory was used to evaluate the chemical structure of the gels. ATR-FTIR spectra were acquired in the 4000-800 cm^{-1} region by averaging 64 scans at a resolution of 4 cm^{-1}.

The viscoelastic properties were determined using the dynamic mechanical analyzer DMA1 (Mettler Toledo, Greifensee, Switzerland) in compression mode. Samples with lateral sizes of 4 mm × 4 mm and a thickness of 1 mm were placed between the clamps above the drive shaft motor. First, a reference test was conducted at room temperature, employing a frequency of 1 Hz and a dynamic force amplitude of 0.1 N. The static preload force was then systematically adjusted within the range of 0.1 N–6.0 N to identify the suitable offset force that would prevent the specimens from slipping out of the clamps. Next, the dynamic force required to obtain noise-free tests was determined by conducting a test at a frequency of 1 Hz, using the previously selected static force as a baseline, and then varying it from 0.1 N to the maximum value of the offset force. These force values, obtained from the preliminary tests, were subsequently utilized to carry out compression tests over a temperature range from −40 °C to 60 °C. These tests were performed at a scanning speed of 3 °C/min and were intended to determine the glass transition temperature and storage modulus of the PVA-based gels.

The density measurements were conducted in accordance with the ASTM D792 [62]. The Density determination kit by Sartorius was used with CPA225D analytical balance with a precision of 0.01 mg and an accuracy of 0.03 mg. Each sample was immersed in a temperature-controlled ethanol bath with a set temperature of 25 °C, ensuring consistency in the measurement conditions. The obtained density values from these measurements were then utilized in the subsequent calculations performed with HZETRN2020. Before conducting the density measurements, the water content of the samples was assessed. Using this information, the remaining input parameters, specifically in terms of atoms per gram (atoms/g), were computed.

3. Results and discussion

3.1. Water content and FTIR analysis of PVA-based gels

PVA gels were investigated to assess the polymer amount that allows to retain higher water contents. Table 2 illustrates the trend in water content for four PVA/BA-T0 gels, which were created using PVA matrices at concentrations of 0.1, 0.2, 0.3, and 0.4 g/mL, over varying periods of water evaporation. The results revealed that the optimal PVA concentration was determined to be 0.3 g/mL, as samples with higher percentages exhibited reduced water content absorption.

Table 3 provides data on the swelling ratio and water content (%) of

Table 2
Water content of PVA/BA-T0 gels with different PVA concentration. Standard deviation of data is below 1 %.

PVA concentration [g/mL]	Water content [%]		
	1 h	**18 h**	**42 h**
0.1	68.6	31.5	11.4
0.2	79.6	49.0	22.4
0.3	82.7	53.9	34.4
0.4	86.1	65.1	27.2

Table 3
Swelling ratio and water content of PVA-based gels obtained by different heat treatments (T0, T1, T2, T2-A). Standard deviation of data is below 1 %.

Samples	Swelling ratio	Water content [%]
PVA-T0	1.23	18.9
PVA/BA-T0	1.24	19.5
PVA/BA-T1	1.18	15.5
PVA/BA-T2	1.15	12.8
PVA/BA-T2-A	1.09	8.2

the PVA-based gels with a polymer concentration of 0.3 g/mL after undergoing different heat treatments (T0, T1, T2, T2-A). Both PVA-T0 and PVA/BA-T0 gels displayed a water content close to 20 %. Notably, the PVA/BA-T0 sample exhibited a slightly higher value, likely attributed to the hydrogen bonding between boron and the PVA chain [63]. The results highlighted that the amount of water retained was influenced by the temperature and duration of the heat treatments. Specifically, it was observed that as the temperature of the heat treatment increased, the water content in the gels decreased. The lowest values were recorded for the PVA/BA-T2 and PVA/BA-T2-A samples, while the PVA/BA-T1 gel displayed higher values due to its shorter duration of heat treatment. The PVA/BA-T2 gel, which underwent a treatment twice as long as PVA/BA-T1, exhibited water content below 13 %. Remarkably, the PVA/BA-T2-A sample, subjected to a 4-month aging process, demonstrated the lowest water content, retaining less than half of its water compared to the PVA/BA-T2 sample that underwent the same heat treatment.

Fig. 3 shows the ATR-FTIR spectra of the PVA-based gels. The spectra of both PVA-T0 and PVA/BA-T0 gels exhibit a high degree of similarity. Specifically, the stretching of the O–H groups at 3284 cm^{-1}, the stretching of the C═O double bond at 1711 cm^{-1}, the H bond at 1643 cm^{-1}, the bending of the C–H bonds in the PVA backbone at 1419 cm^{-1} [64,65], and the asymmetric stretching of the –COO group at 1559 cm^{-1} [66] and the symmetrical stretching of the C–O bond at 1260-1030 cm^{-1} are detected. It can be also observed that the peaks in the spectrum of the PVA/BA hydrogel appear attenuated, especially those around 2927 cm^{-1} corresponding to the asymmetric stretching of the C–H bonds. Furthermore, the introduction of BA into the gel matrix results in the emergence of a new peak at 1335 cm^{-1}, which can be assigned to the antisymmetric vibration of B–O bonds [67]. Importantly, the intensity of

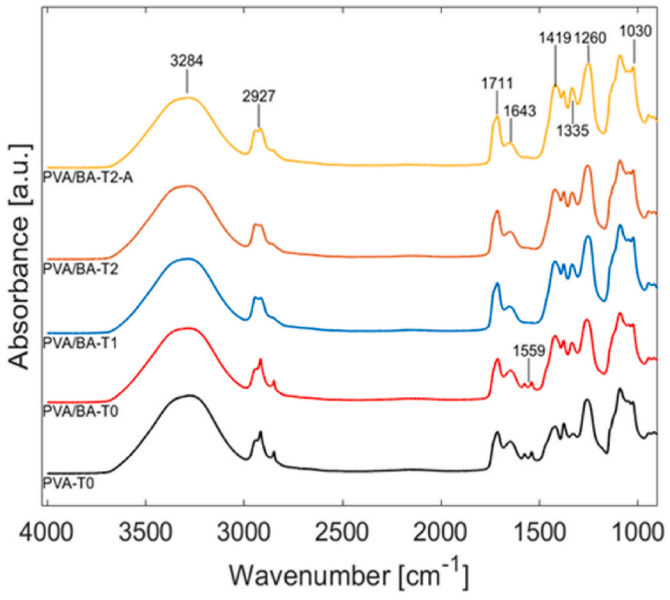

Fig. 3. ATR-FTIR spectra of PVA-based gels obtained by different heat treatments (T0, T1, T2, T2-A).

this peak increases with an extended duration of heat treatment, suggesting the formation of more chemical bonds between PVA and BA over time. This phenomenon is accompanied by a reduction in the intensity of the C–O asymmetric stretching bonds at 1559 cm^{-1} and with the introduction of deformation vibrations of B–O bonds at 1419 cm^{-1}, indicative of alterations in the PVA crystallinity due to the interaction between the polymer matrix and BA [68].

3.2. Dynamic mechanical analysis

Following preliminary tests, the static preload force and the dynamic force amplitude were carefully chosen. Fig. 4 presents a comparison of the storage moduli trend and the static preload forces applied to both the PVA-T0 and PVA/BA-T0 samples for different test times. For both samples, an offset force value of 2.0 N was selected. As detailed in Table 4, the offset force applied during the compression tests is reduced for the gels obtained through higher-temperature treatments (T1, T2, T2-A). Specifically, the offset force is set at 1.5 N for gels with a water content exceeding 10 %, and it is lowered to 1.0 N for gels exhibiting the lowest water content (as observed in the PVA/BA-T2-A type). This reduction in preload force is directly associated with the lower water content. In such cases, the samples display a stiffer behavior and thus require a lower preload force before conducting the test.

As for the dynamic force amplitude analysis, Fig. 5 presents the result of the force sweep tests performed on PVA-T0 and PVA/BA-T0 gels. In this context, the diagrams of the storage modulus (Fig. 5a) and dynamic force amplitude (Fig. 5b) as a function of displacement amplitudes obtained once the offset force values are fixed, are shown. The moduli exhibit a plateau at the initial measurement points, followed by a subsequent decrease in storage modulus alongside an increase in force amplitude. This behavior defines a transition from linear to non-linear elastic region where the ideal value of the force amplitude to use in material characterization is the one that identifies the transition between the two regions. From this analysis, the linear range of the storage modulus in Fig. 5a was determined, ending where the modulus begins to decrease. A displacement of 10 μm was measured for the PVA-T0 sample, which is greater than the one obtained for PVA/BA-T0 samples (equal to 5.5 μm). Fig. 5b enabled us to select a dynamic force corresponding to 0.7 N.

for use in the compression test. Notably, with the same static and dynamic forces applied, the displacement observed in the PVA-T0 sample is twice that of the PVA/BA-T0 sample. This suggests an improvement in mechanical properties attributable to the presence of the BA cross-linker.

The results of the preliminary tests are presented in Table 4, specifically in terms of static and dynamic forces. Notably, it is observed that samples subjected to higher-temperature heat treatments necessitate a force amplitude of 0.6 N to achieve less noisy measurements, while the PVA-T0 and PVA/BA-T0 gels require a force amplitude of 0.7 N. This variation can be attributed to differences in the water content of the gels.

Fig. 6 displays the storage moduli and loss factors obtained from compression tests conducted on both PVA-T0 and PVA/BA-T0 gels. Despite the similar water content in both PVA-based gels, it is evident that the PVA/BA-T0 gel exhibits a storage modulus approximately two times higher than that of pure PVA-T0, indicating superior mechanical performance in the presence of BA. As depicted in Fig. 6a, at room temperature, the elastic modulus for PVA/BA-T0 is measured at 11.53 MPa, while for PVA-T0, it registers at 5.52 MPa. These results are indicative of the presence of bonds between the polymer chain and the crosslinker [52]. Furthermore, the analysis of loss factors displayed in Fig. 6b, reveals glass transition values of approximately −6.5 °C for PVA-T0 and 4.8 °C for PVA/BA-T0. These glass transition temperatures confirm the plasticizing effect of water, consistent with the rubbery and plastic consistency of the samples at room temperature [69].

The plasticizing effect of water becomes evident in Fig. 7, which illustrates the changes in glass transition temperatures (Fig. 7a) and

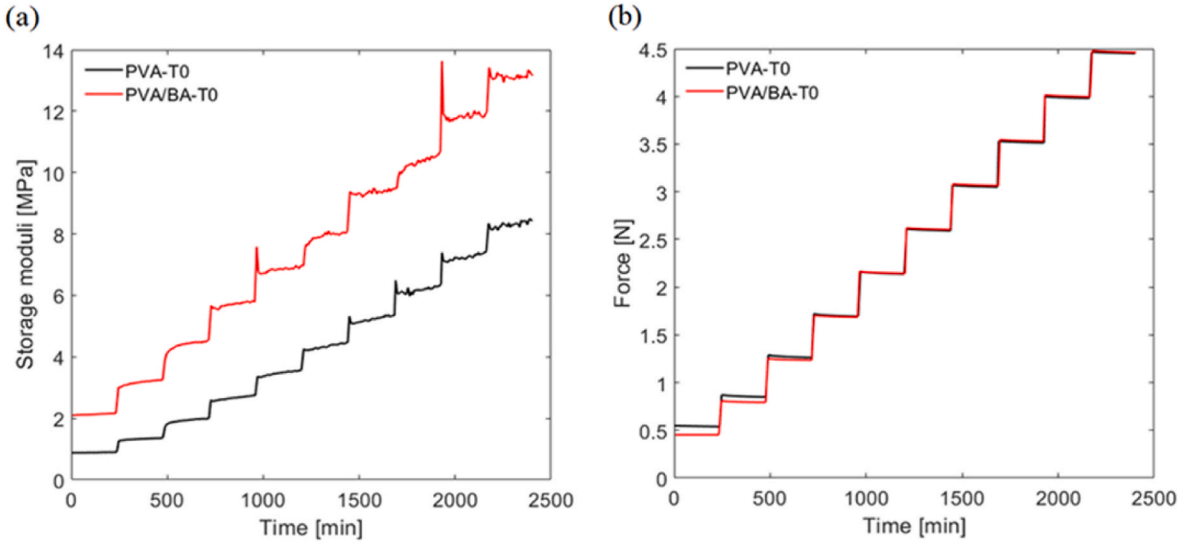

Fig. 4. Comparison of (a) storage moduli and (b) preload static force between PVA-T0 and PVA/BA-T0 samples after offset tests.

Table 4
Static preload and dynamic forces evaluated for compression tests.

Samples	Static preload force [N]	Dynamic amplitude force [N]
PVA-T0	2.0	0.7
PVA/BA-T0	2.0	0.7
PVA/BA-T1	1.5	0.6
PVA/BA-T2	1.5	0.6
PVA/BA-T2-A	1.0	0.6

storage moduli (Fig. 7b) in relation to the water content of PVA/BA gels. As observed, a higher water content results in a reduction of the gels' glass transition temperatures. Conversely, as water evaporates, the modulus decreases, and the glass transition temperature rises, transitioning the material from a plastic to a brittle state. Upon comparing heat-treated samples with those prepared at room temperature, it becomes evident that the decreased water content yields several significant observations. The heat-treated samples generally manifest higher storage moduli, indicating enhanced stiffness and resistance to deformation, potentially extending to the breaking point. Furthermore, heat-treated gels demonstrate elevated glass transition temperatures, implying heightened stiffness and reduced flexibility post-treatment. Moreover, heat-treated samples tend to display a more brittle behavior, typified by a propensity to fracture with minimal plastic deformation prior to failure.

4. Numerical analysis of radiation shielding capability

The radiation shielding capabilities of fabricated gels were investigated using the deterministic transport code developed by NASA at Langley Research Center. The software, HZETRN2020, is designed to calculate radiation transport and shielding effectiveness for spacecraft and astronauts in space environments where they may be exposed to galactic cosmic rays (GCRs) and solar particles events (SPEs). It provides either 1D or 3D solutions to the Boltzmann equation, which describes the behavior of particles as they move through a medium. The code uses approximations and simplifications to make the calculations computationally tractable while maintaining reasonable accuracy. This software is valuable for designing spacecraft shielding, assessing astronaut exposure levels during missions, and evaluating the potential risks of

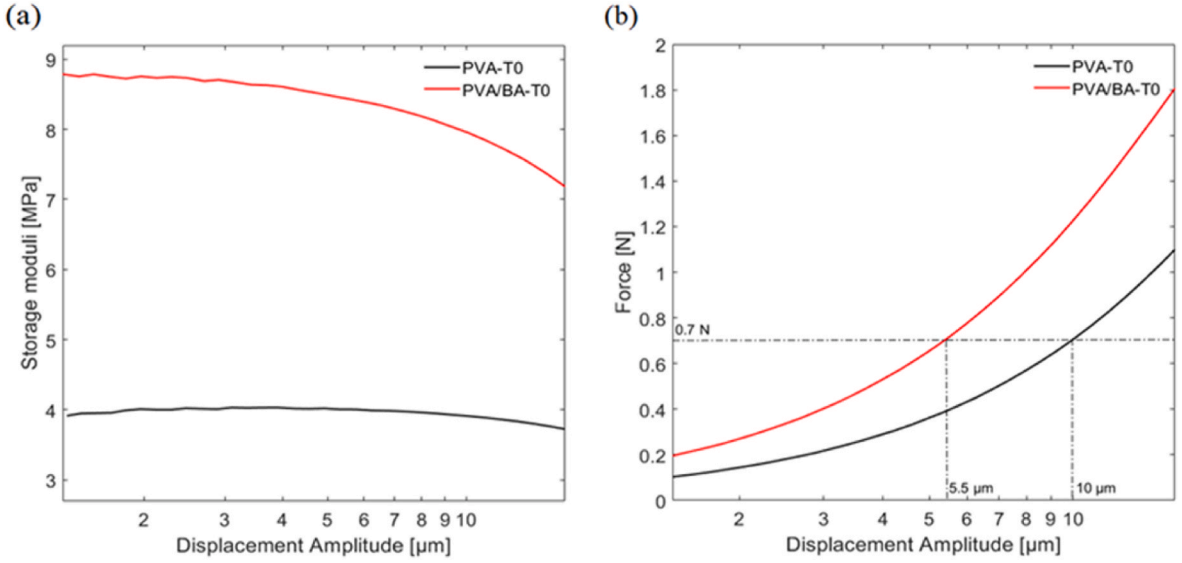

Fig. 5. Comparison of (a) storage moduli and (b) dynamic force amplitude between PVA-T0 and PVA/BA-T0 samples after force sweep tests.

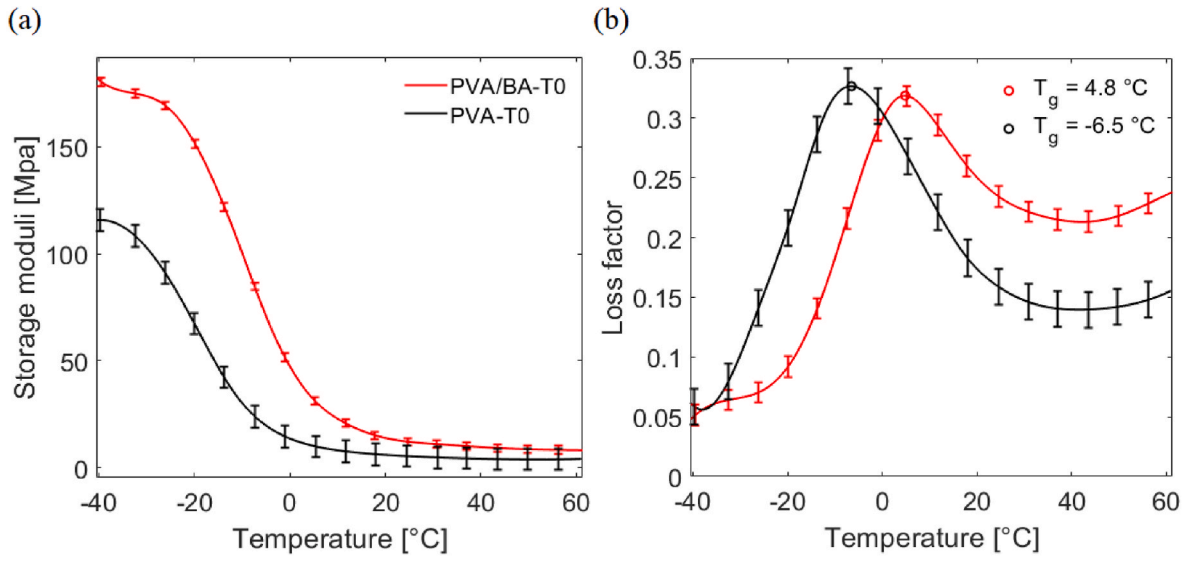

Fig. 6. PVA-T0 and PVA/BA-T0 comparison of (a) storage moduli (b) loss factors.

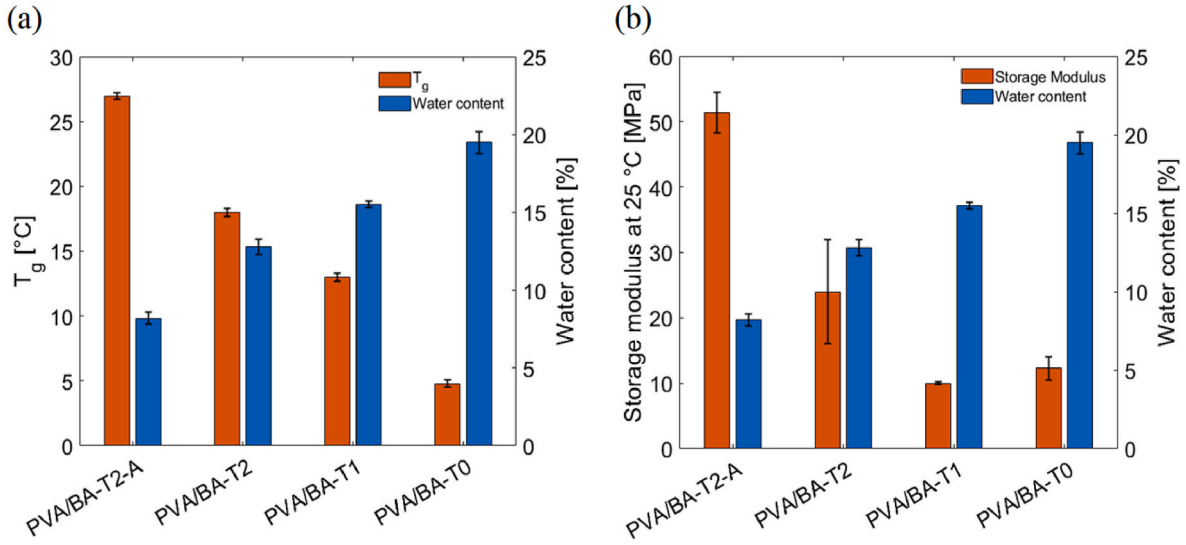

Fig. 7. Comparison of (a) glass transition temperatures and (b) storage moduli at room temperature of the PVA/BA gels.

radiation exposure in space [70]. The code is divided into two modules, which are intended to be used sequentially. The first module is the "cross sections" module, and it utilizes input data related to the shielding material. This module's primary function is to calculate and determine the fragmentation of atoms within the shielding materials based on the input data. Following the execution of the "cross sections" module, the second module, known as the "transport module," comes into play. This module is responsible for transporting radiation through the shielding material. Additionally, it computes various dosimetry quantities in response to the interactions that occur within the material as radiation passes through it. By using these two modules sequentially, the code can effectively model and analyze the behavior of radiation as it interacts with and passes through the chosen shielding materials.

The code generates different key outputs at the end of transport module: dose, fluency, ~~and~~ linear energy transfer (LET), differential and integral flux. In this work, we considered the dose equivalent and the LET. The dose equivalent is the deposited energy per unit mass weighted by an opportune factor depending on the nature of the radiation, and the LET represents the energy lost per unit distance by a charged particle as it passes through a material.

4.1. HZETRN model

The HZETRN requires specific input parameters to accurately model radiation transport through materials and assess shielding effectiveness in the context of space environments. Regarding boundary conditions, it is crucial to provide a description of the radiation fields to which the materials will be exposed. This includes specifying the types of radiation sources or spectra, their energies, and directions of incidence. Regarding material properties, it is necessary to identify the atomic species present in the shielding material by specifying which elements are present and in what relative proportions. Additionally, for each atomic species, the atomic number (Z) and mass number (A) must be provided. The density of the material is also required since it influences the material's mass. Furthermore, the code requires information about the geometry of the shielding setup. This includes details such as the thickness and shape of the shielding material, the arrangement of layers (if applicable), and any void spaces or other structural elements within the shielding.

In this study, the gels were investigated under three different space radiation fields (galactic cosmic rays, solar particle events and radiation in low Earth orbit) at their most detrimental conditions for the spacesuit

materials. To conduct the analysis, both the shielding and response materials were processed as slab geometries, as depicted in Fig. 8. 1D transport solutions (LET and dose equivalent) were calculated using water as response material due to its prevalence in the composition of the human body [71]. The simulations were executed using the Badhwar-O'Neill (BON) 2020 Galactic Cosmic Ray (GCR) model [72] coupled with the classical NUCFRG3 for heavy ion fragmentation [73], the historical Solar Particle Event (SPE) fits from September 1859, and the AP8 model [74] to account for trapped protons in Low Earth Orbit (LEO). Further details on the selection parameters for each environment are provided below.

GCRs originate from outside the solar system and consist of ions traveling at nearly the speed of light. While their particle flux is relatively low compared to SPE sources, they induce intense ionization when passing through matter. This is primarily due to their composition, comprising roughly 85 % hydrogen (protons), 14 % helium, and approximately 1 % high-energy and highly charged ions known as HZE particles [75]. Within HZETRN2020, the GCR environment may be specified by defining the modulation parameter, which describes the state of the heliospheric magnetic field at any given time. It's worth noting that the magnitude of the GCR fluence and energy spectrum are modulated by the 11-year solar cycle [7]. At solar maximum, the increased solar wind emission act as a barrier against GCRs, resulting in reduced overall fluences. For this reason, in our model, we chose to focus on the solar minimum, characterized by $\Phi = 450$ MV. This decision enables us to examine the shielding properties by simulating conditions that are representative of deep space [76]. In this model, HZE particles are categorized into light ions ($Z \leq 2$) and heavy ions ($Z > 2$) to accurately describe fragmentation cross-sections. Additionally, it includes transport models for pions, muons, electrons, positrons, and photons [70,72].

SPEs primarily consist of energetic electrons, protons, and alpha particles that are accelerated by interplanetary shock waves preceding coronal mass ejections and solar flares. Over the years, numerous SPEs have been documented [7]. In this work, we specifically focus on the Carrington event in free space occurred in September 1859 and analyze its capabilities concerning exposure to significantly high particle emissions. This event is particularly noteworthy for its status as the event with the highest fluency, particle flux, and spectral characteristics [77].

When considering the radiation environment in Low Earth Orbit (LEO), we utilized the AP8 MAX trapped proton model [78]. This model accounts for proton anisotropy and pertains to an orbit closely resembling that of the International Space Station (ISS), characterized by an inclination of 51.6° and an altitude of 400 km. At this specific altitude, the predominant contributors to the deposited dose are the trapped protons and the geomagnetically attenuated GCR.

Fig. 9 displays the particle flux boundary conditions for each enviroment. In the GCR environment, the primary charged particles are protons, yet it's essential to address the presence of HZE particles that require shielding. Conversely, in SPE and LEO enviroments, protons are the predominant charged particles. Table 5 contains the input data for the protective materials, providing information about their properties in terms of volumetric density, the number of atomic species, and the relevant mass, charge, and density numbers for each atomic species.

4.1.1. Linear energy transfer

Liquid water was selected as the reference material due to its demonstrated effective shielding capabilities, as validated by experiments conducted as part of the PERSEO project on the International Space Station (ISS) [9]. Fig. 10 illustrates the particle flux as a function of linear energy transfer within a liquid water slab. This analysis aims to assess the stopping power of various shielding materials at thicknesses of 10, 30, and 50 g cm^{-2} in GCR, LEO and SPE environments. As the thickness of the water slab and the deposited energy increase, there is a reduction in particle flux observed across all environments. Generally, LET can be divided into two categories: lower-LET, corresponding to SPEs and LEO, and higher-LET, characteristic of GCRs. Consequently, higher particle flux is observed in GCRs compared to the other two environments [79]. It is worth noting that the particle flux decreases to LET of approximately 4400 keV/μm in GCRs, which is notably higher than the 1200 keV/μm observed in SPEs and LEO. This difference indicates the presence of more damaging charged particles in GCRs, capable of transferring higher energy into the target material.

To compare the shielding effectiveness of PVA and PVA/BA gels, we have presented the particle flux ratio relative to that of liquid water in Figs. 11–13. In the GCR environment, we note minimal deviations from water's performance. In general, when considering low LET, we observe a decrease in shielding effectiveness compared to water, whereas for high LET, the gels exhibit enhanced performance. For a thickness of 10 g cm^{-2}, there is a percentage deviation of less than 2 %. Both gels display inferior shielding properties for LET values above 358 keV/μm, while their performance improves until reaching LET values of 1057 keV/μm. Beyond these thresholds, they once again demonstrate effective shielding capabilities when compared to water. In contrast, when increasing the thickness to 50 g cm^{-2}, the differences become more pronounced. Both gels are 4 % and 6 % less effective than water for LET values above 204 keV/μm until reaching LET values of 1213 keV/μm.

In the LEO environment, both PVA and PVA/BA gels generally

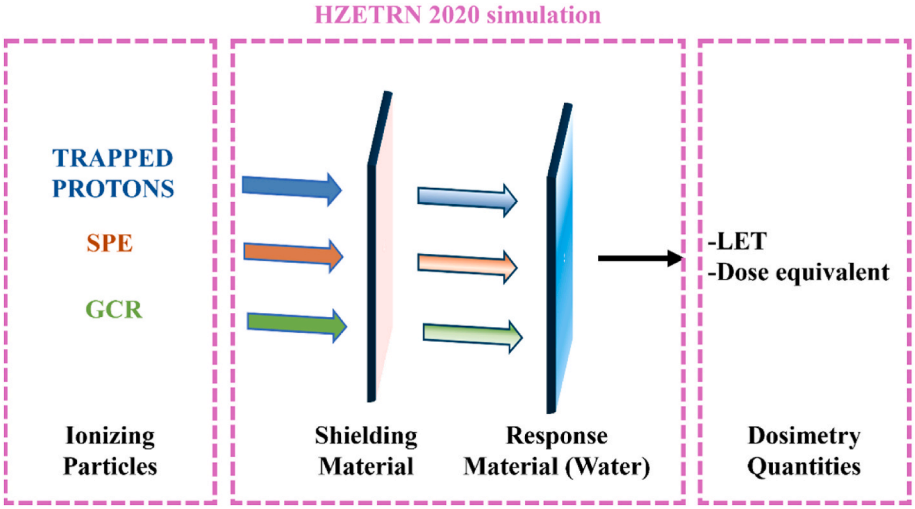

Fig. 8. Representative scheme of numerical simulation.

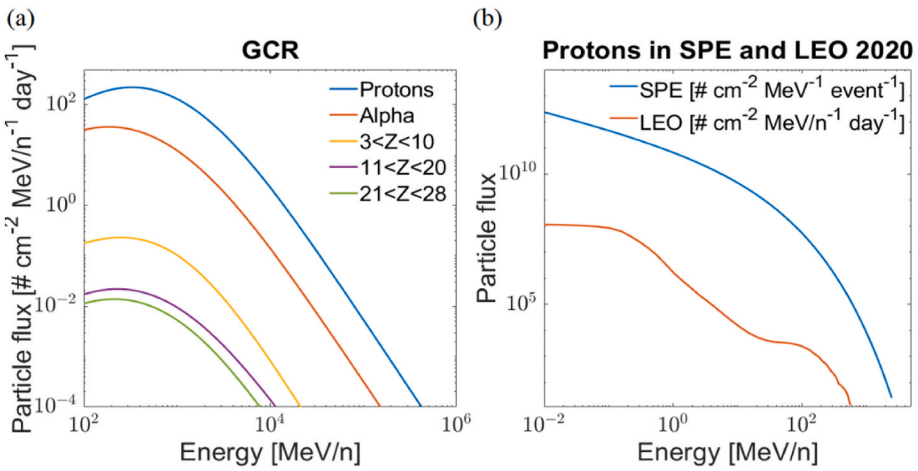

Fig. 9. The ion species' spectra used as boundary conditions for the simulation: (a) CGR spectra in interplanetary space are generated using the updated Badhwar-O'Neill model, specifically for the scenario of minimum solar activity. The primary modulation parameter for this model is φ = 450 MV. (b) SPE conditions associated with the Carrington event of September 1859 in free space are compared to the trapped protons' flux in LEO with an inclination of 51.6° recorded and based on data from the year 2020.

Table 5
Input data for HZETRN2020 code. The unit of the atoms content is atoms $g^{-1} * 10^{22}$.

Shielding Materials	Density [g cm^{-3}]	Atoms •10^{22}					
		Al	$^{12}_{6}C$	$^{1}_{1}H$	$^{16}_{8}O$	$^{10}_{5}B$	$^{11}_{5}B$
Al	2.70	2.2320	/	/	/	/	/
H_2O	1.00	/	/	6.6913	3.3456	/	/
MDPE	0.94	/	4.3015	8.6031	/	/	/
PVA-T0	1.21	/	2.2213	5.7040	1.7413	/	/
PVA/BA-T0	1.24	/	2.0671	5.5828	1.8314	0.00981	0.03924
PVA/BA-T1	1.24	/	2.0964	5.5671	1.8100	0.0099488	0.039795
PVA/BA-T2	1.24	/	2.1895	5.5172	1.7418	0010391	0.041564

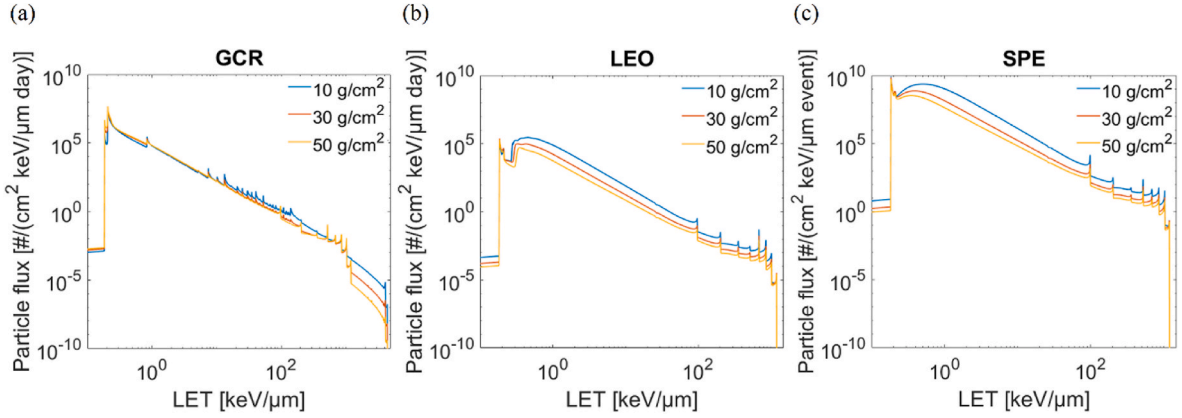

Fig. 10. Particle flux as a function of Linear Energy Transfer (LET) evaluated using a water slab as the shielding material in three distinct environments: (a) galactic cosmic rays, (b) low Earth orbit, and (c) solar particle events.

exhibit slightly lower shielding properties compared to water, except for a specific range of LET values, approximately between 100 and 200 keV/m in which they behave better than water. Interestingly, within this LET range, an increase in thickness corresponds to a decrease in the shielding capabilities of these materials relative to water, as indicated by slightly higher particle flux ratio values. This particular performance characteristic highlights the effectiveness of such gel-based materials for radiation protection in orbit, such as in the environment of the International Space Station (ISS). Since gels are also employed as fabrics in various other application areas [37,80] and the particle flux ratio is close to unity, there is potential to utilize these gels as fabric materials for spacesuits. This innovation could significantly reduce the volume occupied by water connectors in the helmet, torso, limbs, and boots of the spacesuit [20], thereby enhancing astronaut mobility and comfort while maintaining effective radiation shielding.

In the case of SPE, it can be observed that samples subjected to heat treatment (PVA/BA-T1 and PVA/BA-T2) exhibit inferior protective properties compared to those maintained at room temperature (PVA-T0 and PVA/BA-T0). In particular, the particle flux behavior of PVA-T0 and PVA/BA-T0 gels closely resembles each other and is more akin to that of PVA-based gels in the LEO environment. This similarity underscores the effectiveness of gels created at room temperature for shielding against

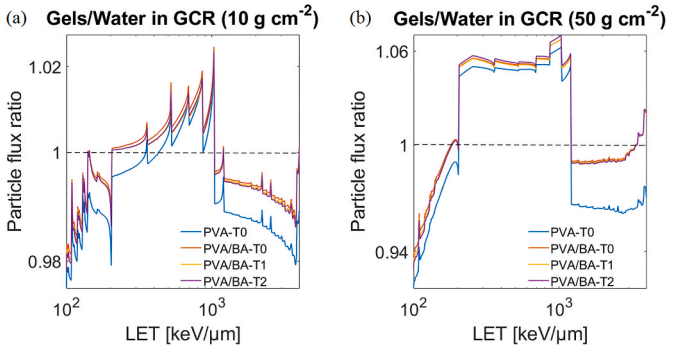

Fig. 11. Particle flux ratio as a function of Linear Energy Transfer (LET) evaluated between PVA-based gels and water as the shielding materials in GCR for slabs' thicknesses of (a) 10 g cm^{-2} and (b) 50 g cm^{-2}.

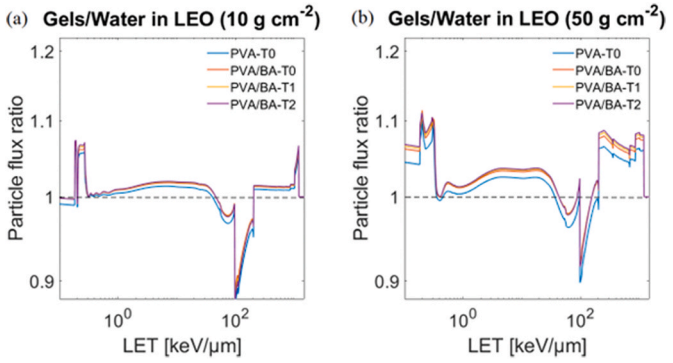

Fig. 12. Particle flux ratio as a function of Linear Energy Transfer (LET) evaluated between PVA-based gels and water as the shielding materials in LEO for slabs' thicknesses of (a) 10 g cm^{-2} (b) 50 g cm^{-2}.

radiation in the context of SPEs.

In general, across all simulated environments, PVA-T0 and PVA/BA-T0 gels exhibit a behavior that closely mirrors that of water itself. Their normalized particle flux trends, when compared to the performance of water, fluctuate around a value of one. This consistency suggests that these gels, particularly those produced at room temperature, offer shielding efficiency comparable to that of water.

4.1.2. Total dose equivalent

Fig. 14 shows the total dose equivalent calculated behind shields made of various materials, including water, aluminum (Al), polyethylene (PE) and cross-linked gels, as a function of material thickness. As documented in existing literature, PE stands out as the most effective shielding material due to its high hydrogen content, while aluminum, a common constituent material of satellites, offers relatively less protective capabilities [81,82]. It can be observed that water and gels overlap, displaying intermediate shielding performance when compared to the other materials. The analysis in GCR environment reveals the most pronounced differences in the protective properties of these materials, highlighting the ability of lightweight hydrogen-rich materials to shield against heavy ion particles.

The shielding performance of water and gels appears to be quite similar. To better appreciate the differences in shielding, we've calculated the percentage deviation from water and presented it in Fig. 15. When comparing the dose fraction behavior to that of water, it is evident that the samples exhibit a trend that hovers around the value of one, closely mirroring that of water. In Fig. 15a, representing the dose fraction in the GCR environment, it is noteworthy that PVA and PVA/BA gels outperform water up to thicknesses of 25 g cm^{-2} and 35 g cm^{-2}, respectively. Among them, pure PVA gels stand out as the most effective

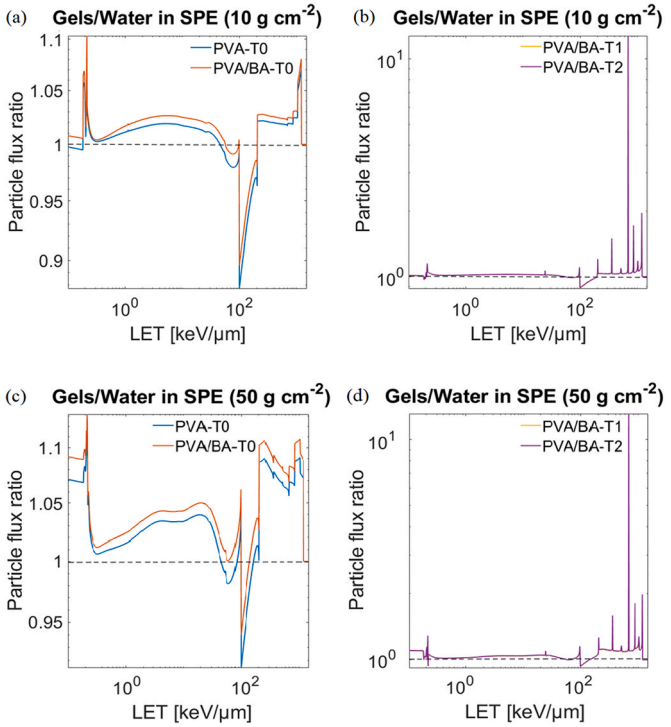

Fig. 13. Particle flux ratio as a function of Linear Energy Transfer (LET) evaluated between PVA-based gels and water as the shielding materials in SPEs for different cases: gels without heat treatments with thicknesses of (a) 10 g cm^{-2} and (b) 50 g cm^{-2}; gels thermally treated with thicknesses of (c) 10 g cm^{-2} and (d) 50 g cm^{-2}.

shielding materials, providing a 1 % improvement over liquid water. On the other hand, gels containing the crosslinking agent show slightly enhanced shielding properties, with heat treatment resulting in an approximate 0.5 % improvement.

In LEO (Fig. 15b), the gels also demonstrate similar behaviors. For lower mass thicknesses, PVA gels display superior shielding properties, while samples containing BA show a slightly lower performance, although overall, their behavior aligns closely with that of water. Heat treatments appear to result in diminished shielding properties, reinforcing the notion that samples created at room temperature show the most promise.

In SPEs, water exhibits better shielding properties than all samples, as evident from Fig. 15c. In general pure PVA gels exhibit slightly better shielding performance than those containing BA. Among the latter, heat treatments lead to a deterioration in shielding properties.

These findings provide valuable insights into the comparative shielding efficiency of different materials under various radiation environments, with gels, particularly pure PVA gels, showing promise as effective shielding materials in certain scenarios.

5. Conclusions

The cross-linked gel samples were fabricated using the PVA polymer with BA, forming interpolymeric hybrid bonds. Samples produced at room temperature (PVA-T0 and PVA/BA-T0) displayed a water content of approximately 20 %, that is notably higher with respect to that of heat-treated samples. In gels containing the crosslinker (BA), the water content was slightly higher due to the presence of B–O bonds between PVA and BA detected by FTIR analysis. Specifically, it is shown that incorporating BA into the gel matrix leads to the emergence of a distinct peak at 1335 cm^{-1} attributed to B–O bonds, along with deformation vibrations of C–H bonds at 1419 cm^{-1}. Dynamic-mechanical compression tests have clearly demonstrated that gels incorporating BA as a

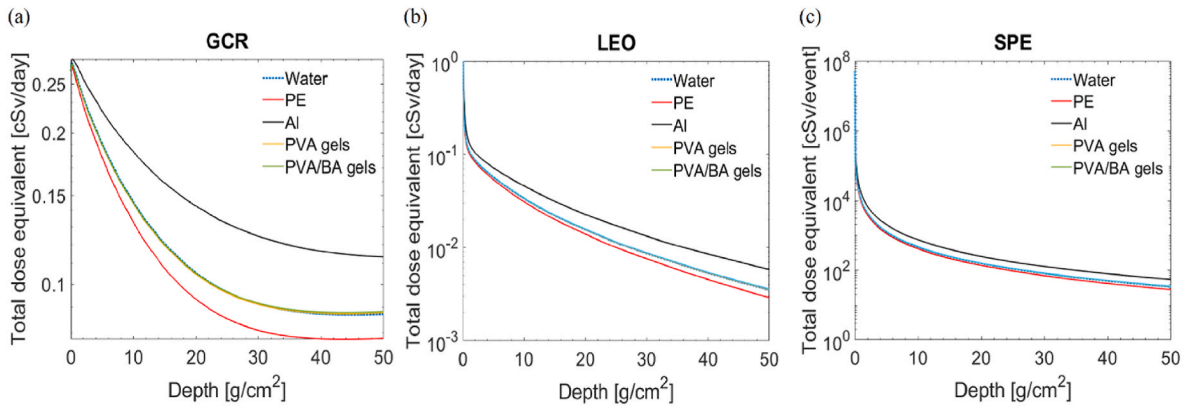

Fig. 14. Total dose equivalent in (a) GCR (b) LEO (c) SPE environments.

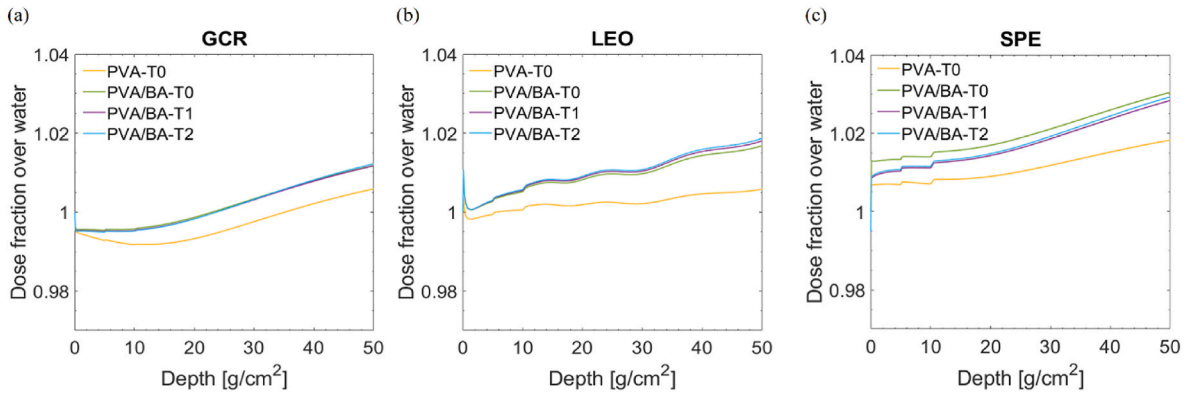

Fig. 15. Ratio between the doses equivalent of PVA-based gels and water evaluated in different enviroments: (a)GCR, (b) LEO, (c) SPEs.

component displayed a substantial increase in storage modulus in comparison to gels made solely from PVA. In fact, the storage modulus in PVA/BA gels was nearly double that of pure PVA gels. This finding strongly suggests that PVA/BA gels exhibit superior mechanical properties, highlighting their enhanced mechanical behavior when contrasted with gels composed exclusively of PVA. When considering specimens that have undergone heat treatments in comparison to those prepared at room temperature, it becomes evident that the lower water content leads to more rigid and less flexible samples. From these findings, it can be inferred that maintaining a water content of approximately 20 % in the gels is essential to ensure a more ductile and flexible behavior, making them better suited for specific applications that require resilience and deformation capacity.

Numerical simulations have consistently indicated that the most effective radiation shielding samples are those created at room temperature. These gels exhibit a normalized particle flux trend that closely mirrors the behavior of water, the reference material. This finding is further supported by the dose equivalent analysis, which demonstrates an improvement over liquid water, particularly for thinner shielding thicknesses. From these results, it can be inferred that PVA-based gels behave similarly to liquid water as shielding materials. This is a significant advantage, as they occupy less space and maintain good mechanical performance.

In summary, PVA/BA gels offer a substantial enhancement in mechanical properties compared to pure PVA gels while providing shielding properties on par with those of liquid water. This combination of improved mechanical strength and effective radiation shielding makes PVA/BA gels a promising candidate for applications in spacesuit, where both radiation protection and flexibility are critical.

Data availability

The data that support the findings of this study are available on request from the corresponding authors.

CRediT authorship contribution statement

Lucia Lambertini: Formal analysis, Investigation, Writing – original draft. **Giuseppe Coccarelli:** Investigation. **Elisa Toto:** Data curation, Validation. **Maria Gabriella Santonicola:** Conceptualization, Methodology, Supervision, Writing – review & editing. **Susanna Laurenzi:** Conceptualization, Methodology, Resources, Supervision, Validation, Writing – review & editing.

Declaration of competing interest

The authors declare that they have no known competing financial interests or personal relationships that could have appeared to influence the work reported in this paper.

Acknowledgements

This work was financially supported by Sapienza University of Rome, Italy(grant numbers MA21916B865F6B61, RM120172B73FC9DC, RM12117A8B3B9A9E).

References

[1] D. Holmberg, Radiation Protection in Space, Umeå Univ., 2010.
[2] A. Gohel, R. Makwana, Multi-layered shielding materials for high energy space radiation, Radiat. Phys. Chem. 197 (2022) 110131, https://doi.org/10.1016/j.radphyschem.2022.110131.

[3] G.G. Shetgaonkar, L. Kumar, Mitigating radiation effects on humans during space Travel: recent developments, in: Y.V. Pathak, M. Araújo Dos Santos, L. Zea (Eds.), Handb. Space Pharm, Springer International Publishing, Cham, 2022, pp. 577–609, https://doi.org/10.1007/978-3-030-05526-4_53.
[4] J.W. Wilson, F.A. Cucinotta, J. Miller, J.L. Shinn, S.A. Thibeault, R.C. Singleterry, L.C. Simonsen, M.H. Kim, Approach and issues relating to shield material design to protect astronauts from space radiation, Mater. Des. 22 (2001) 541–554, https://doi.org/10.1016/S0261-3069(01)00014-0.
[5] M.-H.Y. Kim, Performance Study of Galactic Cosmic Ray Shield Materials, National Aeronautics and Space Administration, Langley Research Center, 1994.
[6] A. Emmanuel, J. Raghavan, Influence of structure on radiation shielding effectiveness of graphite fiber reinforced polyethylene composite, Adv. Space Res. 56 (2015) 1288–1296, https://doi.org/10.1016/j.asr.2015.06.028.
[7] S. Laurenzi, G. de Zanet, M.G. Santonicola, Numerical investigation of radiation shielding properties of polyethylene-based nanocomposite materials in different space environments, Acta Astronaut. 170 (2020) 530–538, https://doi.org/10.1016/j.actaastro.2020.02.027.
[8] F. Zaccardi, E. Toto, M.G. Santonicola, S. Laurenzi, 3D printing of radiation shielding polyethylene composites filled with Martian regolith simulant using fused filament fabrication, Acta Astronaut. 190 (2022) 1–13, https://doi.org/10.1016/j.actaastro.2021.09.040.
[9] G. Baiocco, M. Giraudo, L. Bocchini, S. Barbieri, I. Locantore, E. Brussolo, D. Giacosa, L. Meucci, S. Steffenino, A. Ballario, The PERSEO experience: a water-filled garment prototype for personal radiation protection of astronauts successfully tested on board the international space station, aerotec, Missili Spaz. 99 (2020) 111–114.
[10] S.A. Thibeault, J.H. Kang, G. Sauti, C. Park, C.C. Fay, G.C. King, Nanomaterials for radiation shielding, MRS Bull. 40 (2015) 836–841, https://doi.org/10.1557/mrs.2015.225.
[11] E. Toto, L. Lambertini, S. Laurenzi, M.G. Santonicola, Recent advances and challenges in polymer-based materials for space radiation shielding, Polymers 16 (2024) 382, https://doi.org/10.3390/polym16030382.
[12] W. Zhang, Y. Feng, J.T. Althakafy, Y. Liu, H.M. Abo-Dief, M. Huang, L. Zhou, F. Su, C. Liu, C. Shen, Ultrahigh molecular weight polyethylene fiber/boron nitride composites with high neutron shielding efficiency and mechanical performance, Adv. Compos. Hybrid Mater. 5 (2022) 2012–2020.
[13] F. Zaccardi, E. Toto, S. Rastogi, V. La Saponara, M.G. Santonicola, S. Laurenzi, Impact of proton irradiation on medium density polyethylene/carbon nanocomposites for space shielding applications, Nanomaterials 13 (2023) 1288, https://doi.org/10.3390/nano13071288.
[14] Y. Shang, G. Yang, F. Su, Y. Feng, Y. Ji, D. Liu, R. Yin, C. Liu, C. Shen, Multilayer polyethylene/hexagonal boron nitride composites showing high neutron shielding efficiency and thermal conductivity, Compos. Commun. 19 (2020) 147–153.
[15] V. Pavlenko, N. Cherkashina, R. Yastrebinsky, Synthesis and radiation shielding properties of polyimide/Bi2O3 composites, Heliyon 5 (2019) e01703.
[16] O. Baykara, Ş.G. İrim, A.A. Wis, M.A. Keskin, G. Ozkoc, A. Avcı, M. Doğru, Polyimide nanocomposites in ternary structure:"A novel simultaneous neutron and gamma-ray shielding material,", Polym. Adv. Technol. 31 (2020) 2466–2479.
[17] P.R. De Oliveira, A.K. Sukumaran, L. Benedetti, D. John, K. Stephens, S.-H. Chu, C. Park, A. Agarwal, Novel polyimide-hexagonal boron nitride nanocomposites for synergistic improvement in tribological and radiation shielding properties, Tribol. Int. 189 (2023) 108936.
[18] G.C. Bue, L. Trevino, G. Tsioulos, A. Hanford, Testing of commercial hollow fiber membranes for spacesuit water membrane evaporator. https://doi.org/10.4271/2009-01-2427, 2009: pp. 2009-01–2427.
[19] J. Steele, G. Quinn, C. Watts, J. Makinen, C. Campbell, D. Westheimer, Advanced space suit PLSS 2.0 cooling loop EValuation and PLSS 2.5 recommendations. https://ttu-ir.tdl.org/handle/2346/67619, 2016. (Accessed 24 August 2023).
[20] F.A. Cucinotta, M.R. Shavers, P.B. Saganti, J. Miller, Radiation protection studies of international space station extravehicular activity space suits. https://ntrs.nasa.gov/citations/20040031719, 2003. (Accessed 3 July 2023).
[21] W. Zhen-Wei, L. Dan-lan, C. Peng, Coupling mechanism of spacesuit hip joint and thigh-femur for improved maneuverability of astronauts, Mater. Des. 187 (2020) 108321, https://doi.org/10.1016/j.matdes.2019.108321.
[22] C. Paige, D. Newman, S.J.H. Lombardo, An integrated innovative 3D radiation protection fabric for advanced spacesuits and systems, in: 2020 IEEE Aerosp. Conf., IEEE, Big Sky, 2020, pp. 1–11, https://doi.org/10.1109/AERO47225.2020.9172794. MT, USA.
[23] P. Meti, D.B. Mahadik, K.-Y. Lee, Q. Wang, K. Kanamori, Y.-D. Gong, H.-H. Park, Overview of organic–inorganic hybrid silica aerogels: progress and perspectives, Mater. Des. 222 (2022) 111091, https://doi.org/10.1016/j.matdes.2022.111091.
[24] P. Gupta, B. Singh, A.K. Agrawal, P.K. Maji, Low density and high strength nanofibrillated cellulose aerogel for thermal insulation application, Mater. Des. 158 (2018) 224–236, https://doi.org/10.1016/j.matdes.2018.08.031.
[25] S.C. Gupta, G.L. Baheti, B.P. Gupta, Application of hydrogel system for neutron attenuation, Radiat. Phys. Chem. 59 (2000) 103–107, https://doi.org/10.1016/S0969-806X(00)00189-4.
[26] Y. Osada, J. Ping Gong, Y. Tanaka, Polymer gels, J. Macromol. Sci. Part C 44 (2004) 87–112, https://doi.org/10.1081/MC-120027935.
[27] V.K. Thakur, M.K. Thakur (Eds.), Polymer Gels: Synthesis and Characterization, Springer, Singapore, 2018, https://doi.org/10.1007/978-981-10-6083-0.
[28] A.H. Clark, Structural and mechanical properties of biopolymer gels, in: Food Polym. Gels Colloids, Elsevier, 1991, pp. 322–338, https://doi.org/10.1533/9781845698331.322.
[29] J.D. Ferry, Structure and rheology of fibrin networks, in: O. Kramer (Ed.), Biol. Synth. Polym. Netw, Springer Netherlands, Dordrecht, 1988, pp. 41–55, https://doi.org/10.1007/978-94-009-1343-1_2.
[30] K. Bialik-Waś, E. Królicka, D. Malina, Impact of the type of crosslinking agents on the properties of modified sodium alginate/poly(vinyl alcohol) hydrogels, Molecules 26 (2021), https://doi.org/10.3390/molecules26082381.
[31] M. Bercea, Bioinspired hydrogels as platforms for life-science applications: challenges and opportunities, Polymers 14 (2022) 2365.
[32] M. Bercea, Self-healing behavior of polymer/protein hybrid hydrogels, Polymers 14 (2021) 130, https://doi.org/10.3390/polym14010130.
[33] M. Chelu, A.M. Musuc, Polymer gels: classification and recent developments in biomedical applications, Gels 9 (2023) 161, https://doi.org/10.3390/gels9020161.
[34] M.I. Baker, S.P. Walsh, Z. Schwartz, B.D. Boyan, A review of polyvinyl alcohol and its uses in cartilage and orthopedic applications, J. Biomed. Mater. Res. B Appl. Biomater. 100B (2012) 1451–1457, https://doi.org/10.1002/jbm.b.32694.
[35] G. Ciarleglio, S. Vella, E. Toto, M.G. Santonicola, Emulsion-based multi-responsive microspheres for the delivery of lipophilic Ozoile, Ceram. Int. (2023), https://doi.org/10.1016/j.ceramint.2022.12.095.
[36] G. Ciarleglio, E. Toto, M.G. Santonicola, Conductive and thermo-responsive composite hydrogels with poly(N-isopropylacrylamide) and carbon nanotubes fabricated by two-step photopolymerization, Polymers 15 (2023) 1022, https://doi.org/10.3390/polym15041022.
[37] M. Bercea, L.-M. Gradinaru, S. Morariu, I.-A. Plugariu, R.V. Gradinaru, Tailoring the properties of PVA/HPC/BSA hydrogels for wound dressing applications, React. Funct. Polym. 170 (2022) 105094, https://doi.org/10.1016/j.reactfunctpolym.2021.105094.
[38] M.A. Radwan, O.H. Al-Sweasy, H.A. Elazab, Preparation of hydrogel based on acryl amide and investigation of different factors affecting rate and amount of absorbed water, Agric. Sci. 8 (2017) 161.
[39] L. Voorhaar, R. Hoogenboom, Supramolecular polymer networks: hydrogels and bulk materials, Chem. Soc. Rev. 45 (2016) 4013–4031.
[40] M. Rizwan, S.R. Gilani, A.I. Durani, S. Naseem, Materials diversity of hydrogel: synthesis, polymerization process and soil conditioning properties in agricultural field, J. Adv. Res. 33 (2021) 15–40.
[41] Z.W. Abdullah, Y. Dong, I.J. Davies, S. Barbhuiya, PVA, PVA blends, and their nanocomposites for biodegradable packaging application, Polym.-Plast. Technol. Eng. 56 (2017) 1307–1344.
[42] A. Kumar, S.S. Han, PVA-based hydrogels for tissue engineering: a review, Int. J. Polym. Mater. Polym. Biomater. 66 (2017) 159–182, https://doi.org/10.1080/00914037.2016.1190930.
[43] Y. Chen, J. Li, J. Lu, M. Ding, Y. Chen, Synthesis and properties of Poly(vinyl alcohol) hydrogels with high strength and toughness, Polym. Test. 108 (2022) 107516, https://doi.org/10.1016/j.polymertesting.2022.107516.
[44] Y. Chen, C. Jiao, X. Peng, T. Liu, Y. Shi, M. Liang, H. Wang, Biomimetic anisotropic poly(vinyl alcohol) hydrogels with significantly enhanced mechanical properties by freezing–thawing under drawing, J. Mater. Chem. B 7 (2019) 3243–3249, https://doi.org/10.1039/C9TB00372J.
[45] N.A. Peppas, E.W. Merrill, Crosslinked poly(vinyl alcohol) hydrogels as swollen elastic networks, J. Appl. Polym. Sci. 21 (1977) 1763–1770, https://doi.org/10.1002/app.1977.070210704.
[46] H. Zhang, H. Xia, Y. Zhao, Poly(vinyl alcohol) hydrogel can autonomously self-heal, ACS Macro Lett. 1 (2012) 1233–1236, https://doi.org/10.1021/mz300451r.
[47] S.A. Bernal-Chávez, A. Romero-Montero, H. Hernández-Parra, S.I. Peña-Corona, M. L. Del Prado-Audelo, S. Alcalá-Alcalá, H. Cortés, L. Kiyekbayeva, J. Sharifi-Rad, G. Leyva-Gómez, Enhancing chemical and physical stability of pharmaceuticals using freeze-thaw method: challenges and opportunities for process optimization through quality by design approach, J. Biol. Eng. 17 (2023) 35, https://doi.org/10.1186/s13036-023-00353-9.
[48] B.S. Chee, G. Goetten De Lima, D.M. Devine, M.J.D. Nugent, Investigation of the effects of orientation on freeze/thawed Polyvinyl alcohol hydrogel properties, Mater. Today Commun. 17 (2018) 82–93, https://doi.org/10.1016/j.mtcomm.2018.08.005.
[49] S. Verma, S.S. Amritphale, S. Das, Preparation and characterization of novel, non-toxic, radiation shielding, self-healing smart gel, Cellulose 24 (2017) 2953–2965, https://doi.org/10.1007/s10570-017-1301-2.
[50] A. Marini, L. Lazzeri, M.G. Cascone, R. Ciolini, L. Tana, F. d'Errico, Fricke gel dosimeters with low-diffusion and high-sensitivity based on a chemically cross-linked PVA matrix, Radiat. Meas. 106 (2017) 618–621, https://doi.org/10.1016/j.radmeas.2017.02.012.
[51] S. Kudo, E. Otsuka, A. Suzuki, Swelling behavior of chemically crosslinked PVA gels in mixed solvents, J. Polym. Sci., Part B: Polym. Phys. 48 (2010) 1978–1986, https://doi.org/10.1002/polb.22076.
[52] R.V. Gadhave, P.A. Mahanwar, P.T. Gadekar, Study of cross-linking between boric acid and different types of polyvinyl alcohol adhesive, Open J. Polym. Chem. 9 (2019) 16–26, https://doi.org/10.4236/ojpchem.2019.91002.
[53] N. Wang, L. Zhao, C. Zhang, L. Li, Water states and thermal processability of boric acid modified poly(vinyl alcohol), J. Appl. Polym. Sci. 133 (2016), https://doi.org/10.1002/app.43246 n/a-n/a.
[54] T. Miyazaki, Y. Takeda, S. Akane, T. Itou, A. Hoshiko, K. En, Role of boric acid for a poly (vinyl alcohol) film as a cross-linking agent: melting behaviors of the films with boric acid, Polymer 51 (2010) 5539–5549, https://doi.org/10.1016/j.polymer.2010.09.048.
[55] I.Yu Prosanov, S.T. Abdulrahman, S. Thomas, N.V. Bulina, K.B. Gerasimov, Complex of polyvinyl alcohol with boric acid: structure and use, Mater. Today Commun. 14 (2018) 77–81, https://doi.org/10.1016/j.mtcomm.2017.12.012.

[56] S. Zhang, D. Wei, X. Xu, Y. Guan, Transparent, high-strength, and antimicrobial polyvinyl alcohol/boric acid/poly hexamethylene guanidine hydrochloride films, Coatings 13 (2023) 1115.
[57] X. Hong, J. He, L. Zou, Y. Wang, Y.V. Li, Preparation and characterization of high strength and high modulus PVA fiber via dry-wet spinning with cross-linking of boric acid, J. Appl. Polym. Sci. 138 (2021) 51394, https://doi.org/10.1002/app.51394.
[58] J. Chen, Y. Li, Y. Zhang, Y. Zhu, Preparation and characterization of graphene oxide reinforced PVA film with boric acid as crosslinker, J. Appl. Polym. Sci. 132 (2015).
[59] H. Wang, T. Shyr, M. Hu, The elastic property of polyvinyl alcohol gel with boric acid as a crosslinking agent, J. Appl. Polym. Sci. 74 (1999) 3046–3052.
[60] H.-H. Wang, T.-W. Shyr, M.-S. Hu, Thermal and rheological properties of poly (vinyl alcohol) gel with boric acid as a crosslinking agent, J. Appl. Polym. Sci. 73 (1999) 2219–2226, https://doi.org/10.1002/(SICI)1097-4628(19990912)73:11<2219::AID-APP19>3.0.CO;2-G.
[61] A.S. Kipcak, O. Ismail, I. Doymaz, S. Piskin, Modeling and investigation of the swelling kinetics of acrylamide-sodium acrylate hydrogel, J. Chem. 2014 (2014) 1–8, https://doi.org/10.1155/2014/281063.
[62] D20 Committee, Test Methods for Density and Specific Gravity (Relative Density) of Plastics by Displacement, ASTM International, n.d. https://doi.org/10.1520/D0792-00..
[63] S. Rahmani, A. Olad, Z. Rahmani, Preparation of self-healable nanocomposite hydrogel based on Gum Arabic/gelatin and graphene oxide: study of drug delivery behavior, Polym. Bull. (2022), https://doi.org/10.1007/s00289-022-04247-6.
[64] H.S. Mansur, C.M. Sadahira, A.N. Souza, A.A.P. Mansur, FTIR spectroscopy characterization of poly (vinyl alcohol) hydrogel with different hydrolysis degree and chemically crosslinked with glutaraldehyde, Mater. Sci. Eng. C 28 (2008) 539–548, https://doi.org/10.1016/j.msec.2007.10.088.
[65] J. Coates, Interpretation of Infrared Spectra, a Practical Approach, 2000.
[66] Z. Dai, J. Deng, L. Ansaloni, S. Janakiram, L. Deng, Thin-film-composite hollow fiber membranes containing amino acid salts as mobile carriers for CO2 separation, J. Membr. Sci. 578 (2019) 61–68.
[67] P.-Y. Pennarun, P. Jannasch, S. Papaefthimiou, N. Skarpentzos, P. Yianoulis, High coloration performance of electrochromic devices assembled with electrolytes based on a branched boronate ester polymer and lithium perchlorate salt, Thin Solid Films 514 (2006) 258–266.
[68] I. Yanase, R. Ogawara, H. Kobayashi, Synthesis of boron carbide powder from polyvinyl borate precursor, Mater. Lett. 63 (2009) 91–93, https://doi.org/10.1016/j.matlet.2008.09.012.
[69] R. Hodge, T. Bastow, G. Edward, G. Simon, A. Hill, Free volume and the mechanism of plasticization in water-swollen poly (vinyl alcohol), Macromolecules 29 (1996) 8137–8143.
[70] T.C. Slaba, J.W. Wilson, C.M. Werneth, K. Whitman, Updated deterministic radiation transport for future deep space missions, Life Sci. Space Res. 27 (2020) 6–18, https://doi.org/10.1016/j.lssr.2020.06.004.
[71] ICRP, International Commission on Radiological Protection. Recommendations of the International Commission on Radiological Protection, 60, ICRP Publication, 1991.
[72] T.C. Slaba, K. Whitman, The badhwar-O'neill 2020 GCR model, Space Weather 18 (2020), https://doi.org/10.1029/2020SW002456.
[73] Adamczyk, A.M., Norman, R.B., Sriprisan, S.I., Townsend, L.W., Norbury, J.W., Blattnig, S.R., Slaba, T.C., NUCFRG3: Light ion Improvements to the Nuclear Fragmentation Model. Nuc. Instr. Meth. A 678: 21-32; 2012.
[74] D.M. Sawyer, J.I. Vette, AP-8 Trapped Proton Environments for Solar Maximum and Solar Minimum, NSSDC/WDC-A-R&S 76-06 (1976).
[75] A.C. Tribble, The Space Environment: Implications for Spacecraft Design-Revised and Expanded Edition, Princeton University Press, 2020.
[76] P.M. O'Neill, Badhwar–O'Neill galactic cosmic ray model update based on advanced composition explorer (ACE) energy spectra from 1997 to present, Adv. Space Res. 37 (2006) 1727–1733, https://doi.org/10.1016/j.asr.2005.02.001.
[77] L.W. Townsend, D.L. Stephens, J.L. Hoff, E.N. Zapp, H.M. Moussa, T.M. Miller, C. E. Campbell, T.F. Nichols, The Carrington event: possible doses to crews in space from a comparable event, Adv. Space Res. 38 (2006) 226–231, https://doi.org/10.1016/j.asr.2005.01.111.
[78] F.F. Badavi, K.J. West, J.E. Nealy, J.W. Wilson, B.L. Abrahms, N.J. Luetke, A dynamic/anisotropic low earth orbit (LEO) ionizing radiation model. https://ntrs.nasa.gov/citations/20070004574, 2006. (Accessed 23 June 2023).
[79] G. Dietze, D.T. Bartlett, D.A. Cool, F.A. Cucinotta, X. Jia, I.R. McAulay, M. Pelliccioni, V. Petrov, G. Reitz, T. Sato, ICRP publication 123: assessment of radiation exposure of astronauts in space, Ann. ICRP 42 (2013) 1–339, https://doi.org/10.1016/j.icrp.2013.05.004.
[80] W.R.K. Illeperuma, P. Rothemund, Z. Suo, J.J. Vlassak, Fire-resistant hydrogel-fabric laminates: a simple concept that may save lives, ACS Appl. Mater. Interfaces 8 (2016) 2071–2077, https://doi.org/10.1021/acsami.5b10538.
[81] A. Gohel, R. Makwana, B. Soni, Evaluating shielding materials for high energy space radiation, IOP Conf. Ser. Mater. Sci. Eng. 1221 (2022) 012003, https://doi.org/10.1088/1757-899X/1221/1/012003.
[82] R.C. Singleterry, Radiation engineering analysis of shielding materials to assess their ability to protect astronauts in deep space from energetic particle radiation, Acta Astronaut. 91 (2013) 49–54, https://doi.org/10.1016/j.actaastro.2013.04.013.